

PAPER

SpaDiT: Diffusion Transformer for Spatial Gene Expression Prediction using scRNA-seq

Xiaoyu Li,^{1#} Fangfang Zhu^{2#} and Wenwen Min^{1*}¹the School of Information Science and Engineering, Yunnan University, 650091, Kunming, Yunnan, China and ²College of Nursing Health Sciences, Yunnan Open University, 650599, Kunming, China*Corresponding author: minwenwen@ynu.edu.cn and #Co-first authors

FOR PUBLISHER ONLY Received on Date Month Year; revised on Date Month Year; accepted on Date Month Year

Abstract

The rapid development of spatial transcriptomics (ST) technologies is revolutionizing our understanding of the spatial organization of biological tissues. Current ST methods, categorized into next-generation sequencing-based (seq-based) and fluorescence in situ hybridization-based (image-based) methods, offer innovative insights into the functional dynamics of biological tissues. However, these methods are limited by their cellular resolution and the quantity of genes they can detect. To address these limitations, we propose SpaDiT, a deep learning method that utilizes a diffusion generative model to integrate scRNA-seq and ST data for the prediction of undetected genes. By employing a Transformer-based diffusion model, SpaDiT not only accurately predicts unknown genes but also effectively generates the spatial structure of ST genes. We have demonstrated the effectiveness of SpaDiT through extensive experiments on both seq-based and image-based ST data. SpaDiT significantly contributes to ST gene prediction methods with its innovative approach. Compared to eight leading baseline methods, SpaDiT achieved state-of-the-art performance across multiple metrics, highlighting its substantial bioinformatics contribution.

Key words: diffusion model, spatial transcriptomics data, scRNA-seq data, Transformer

Introduction

Single-cell RNA sequencing (scRNA-seq) can represent the entire transcriptome of a specific cell in an organ, providing an excellent perspective for in-depth study of various behaviors and mechanisms between cells [1]. However, since scRNA-seq must undergo sample tissue dissociation, it also leads to the inability of scRNA-seq to capture the spatial distribution and spatial information of cells, which is often crucial for understanding the complex physiological processes between cells [2]. Therefore, spatial transcriptomics (ST) has emerged as an advanced technology that can retain spatial location information while measuring gene expression in tissue or cell samples [3]. This technology enables researchers to parse the spatial distribution of gene expression in tissues, enhancing the understanding of cell types, functions, interactions, and key details in development, disease, and biological processes.

At present, ST technology can be mainly divided into two categories: Based on next-generation sequencing technology (seq-based): such as 10x Visium [4], Slide-seq [5] and Stereo-seq [6], transcriptome-wide gene expression within a spatial point can be detected. Fluorescence in situ hybridization (image-based): such as seqFish [7] and MERFISH [8], can measure thousands of genes at the resolution of single cells, but they usually lack full transcriptome coverage, resulting in only a few hundred genes in actual sequencing. Although

these two technologies can detect gene expression in the whole transcriptome range, their capture rate is low due to their resolution [9, 10]. The current solution mainly focuses on increasing the capture rate and predicting uncaptured genes by using scRNA-seq data to enhance ST data to improve its resolution [11, 12, 13].

In recent years, a variety of methods have been proposed to use scRNA-seq data to improve the resolution of ST data and predict uncaptured genes. These methods, such as Tangram [14], scVI [15], SpaGE [16], stplus [17], SpaOTsc [18], novoSpaRc [19], SpatialScope [20], stDiff [21]. They all assume that scRNA-seq data and ST data have similar expression distributions, and they identify the similarity between scRNA-seq cells and ST cells by detecting the expression patterns of shared genes. Then, these methods use similar scRNA-seq cells to predict the unmeasured part of ST data. However, due to the sparse nature of scRNA-seq and ST data, and the reliance on common genes to calculate similarity, this poses a huge challenge to how to align the two data. In addition, simply using scRNA-seq as a reference for ST data prediction is difficult to avoid introducing batch bias of scRNA, which increases the difficulty of predicting unknown genes [22].

In this paper, we introduce a novel method named SpaDiT, which uses a conditional diffusion model to understand and generate unmeasured gene expression in ST data. Although

Table 1. The list of ten paired scRNA-seq and spatial transcriptomic datasets. The first five ST datasets are image-based, the next five datasets are sequencing-based. HPR: hypothalamic preoptic region; PMC: primary motor cortex.

Datasets	Tissue	GEO ID	Platform		Number of Cells/Spots		Number of Genes		Prepro. Cells/Spots		Prepro. Genes		Dropout Rate	
			SC	ST	SC (Cells)	ST (Spots)	SC (Genes)	ST (Genes)	SC (Cells)	ST (Spots)	SC (Genes)	ST (Genes)	SC	ST
MH [26]	mouse hippocampus	GSE158450	10X Chromium	seqFish	8596	3585	16384	249	8584	3585	1260	249	80.3%	6.3%
MHPR [27]	mouse HPR	GSE113576	10X Chromium	MERFISH	31299	4975	18646	154	31297	4975	1939	153	73.7%	62.2%
ML [28]	mouse liver	GSE109774	Smart-seq2	seqFISH	981	2177	17533	19532	887	2177	2279	569	73.2%	75.4%
MG [28]	mouse gastrulation	GSE15677	10X Chromium	seqFISH	4651	8425	19103	351	4651	8425	1945	345	58.6%	74.1%
MVC [29]	mouse visual cortex	-	Smart-seq	STARmap	14249	1549	34041	1020	14249	1549	3774	844	58.2%	76.2%
MHM [30]	mouse hindlimb muscle	GSE161318	10X Chromium	10X Visium	4816	995	15460	33217	4809	995	1667	416	80.3%	68.9%
HBC [31]	human breast cancer	CID3586	10X Chromium	10X Visium	6178	4784	21164	28402	6143	4784	625	125	76.6%	70.6%
ME [32]	mouse embryo	GSE160137	10X Chromium	10X Visium	3415	198	19374	53574	3415	198	2163	540	61.1%	62.3%
MPMC [33]	mouse PMC	-	10X Chromium	10X Visium	3499	9852	24340	24518	3499	9852	2544	636	70.6%	81.7%
MC [34]	mouse cerebellum	SCP948	10X Chromium	Slide-seqV2	26252	41674	24409	23264	26252	41674	822	205	79.5%	83.9%

diffusion models have made significant contributions in the field of computer vision and have shown excellent performance in the field of protein or drug generation [23, 24, 25], their application in genomics is still relatively limited. The goal of SpaDiT is to utilize scRNA-seq as a prior input in the diffusion model to help the model understand the relationship between gene expressions, thereby guiding the model to generate genes that are not measured in ST data. SpaDiT utilizes genes in single cells as unique identifiers by incorporating them in the diffusion model along with the corresponding genes in ST, and employs the Transformer-based diffusion model to enhance the model’s prediction accuracy of specific genes.

We conduct a comprehensive performance evaluation on 10 ST datasets based on different sequencing technologies, different tissues, and different sample sizes, and compare them with the current state of the art (SOTA) methods. The results show that our model achieves the best performance on all five evaluation indicators, and the correlation between predicted gene expression and actual gene expression shows the best accuracy. This shows that SpaDiT can effectively make predictions when predicting unmeasured gene expression in ST data. In addition, the genes predicted by our model have a high spatial similarity with the genes in the actual ST data. For the spatial expression patterns of each data set, our model can accurately predict and clearly divide the spatial boundaries. This demonstrates SpaDiT’s ability to predict ST data gene expression and provide subsequent analysis.

Materials and methods

Datasets and pre-processing

In this paper, we collected ten benchmark datasets (scRNA sequencing and spatial transcriptomics data) from different tissues of various organisms. As illustrated in Table 1, these datasets originate from various biological organizations and utilize differing sequencing platforms and technologies. They also vary in sample sizes, number of spatially measured genes, and missing data rates. Specifically, the sequencing platforms for single-cell data in these datasets include 10X Chromium, Smart-seq, and Smart-seq2. For spatial transcriptomics data, the platforms are seqFISH, MERFISH, 10X Visium, STARmap, and Slide-seqV2. These datasets are derived from different biological tissues, primarily from mouse and human breast cancer tissue sections.

For the implementation of SpaDiT, we adhered to the data preprocessing protocols as established in prior studies [35]. More specifically, we first removed genes with no expression from both the single-cell and spatial transcriptomics datasets. Subsequently, we screened the remaining genes to identify those that were highly expressed, using criteria based on the number of genes in each dataset.

We partitioned the processed data into training, validation, and test sets with ratios of 7:2:1, respectively. These subsets are mutually independent, with the test set being strictly separate from the training set. All reported results were derived solely from evaluations on the test set.

The architecture of SpaDiT

SpaDiT is a conditional diffusion-based deep generative model that enhances spatial transcriptomics data by leveraging single-cell RNA sequencing (scRNA-seq) data as prior information, aiming to accurately predict the expression of unmeasured or unknown genes. As illustrated in the Figure 1, SpaDiT takes two types of input data: a gene expression matrix from spatial transcriptomics data and another from scRNA-seq data. Utilizing a conditional diffusion model, SpaDiT uses scRNA-seq data as a conditioning factor to guide the model through the diffusion and denoising processes, thereby generating the targeted gene expression profiles for the spatial transcriptomic data. The SpaDiT architecture comprises three key modules: the Latent Embedding module for processing spatial transcriptomic data, the Condition Embedding module for processing scRNA-seq data, and the core network architecture: Diffusion with Transformer, which facilitates the integration and generation of data. In the following sections, we will introduce the main modules of SpaDiT.

Latent Embedding in SpaDiT

In the proposed SpaDiT, the latent embedding module is crucial. Instead of operating directly on real data, we work within an efficient, low-dimensional latent space, which is better suited for likelihood-based generative models. Therefore, we utilize an encoder to map the high-dimensional input data to a low-dimensional representation, and we train the diffusion model within this latent space.

Notably, our proposed method involves two types of data input: spatial transcriptomics data (X_{st}) and scRNA-seq data (X_{sc}). The genes in X_{sc} are divided into shared genes (G_{share}) with spatial transcriptomics data and unique genes (G_{unique}). For the input of Latent Embedding, we define it as follows: for each sample (i.e., gene) $x_{st}^i \in X_{st}$ in the spatial transcription data, we integrate it with the scRNA-seq data $x_{sc}^i \in X_{sc}$, where x_{st}^i and x_{sc}^i in G_{share} are utilized as inputs. In latent embedding, we employ a simple feed-forward network to project x_{st}^i and x_{sc}^i into the same dimensional space, concatenating the projected \hat{x}_{st}^i and \hat{x}_{sc}^i as the output of the latent embedding, that is, $x_\phi = \hat{x}_{st}^i \oplus \hat{x}_{sc}^i$.

Condition Embedding in SpaDiT

The condition embedding module leverages scRNA-seq data as a conditioning factor in our model, integrating it into the diffusion process to guide the model in generating the

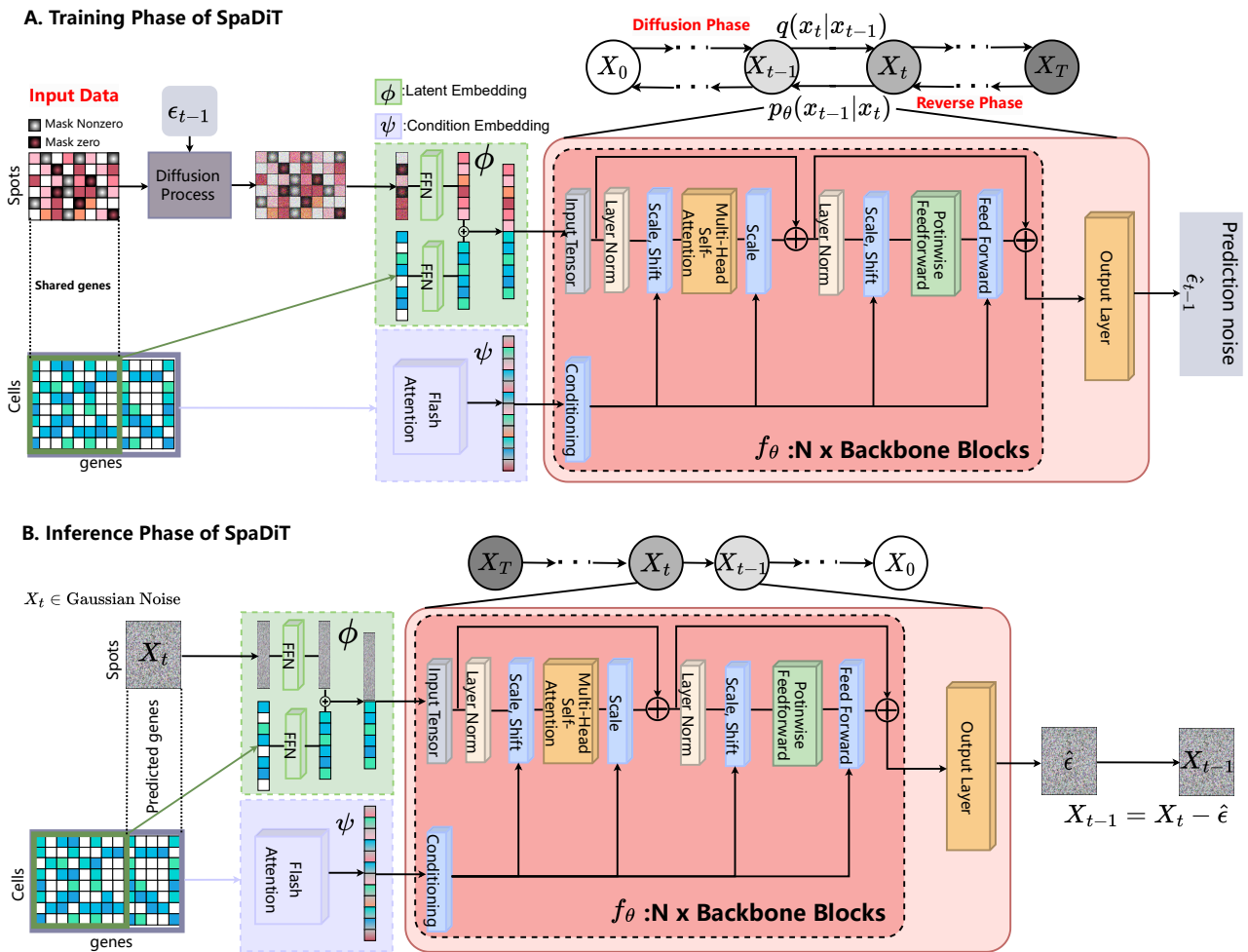


Fig. 1. The architecture of SpaDiT. There are three parts in total: latent embedding, conditional embedding and network backbone. (A) is the training process where each gene is considered as a sample, and (B) is the inference process.

required gene expression. Given that scRNA-seq data is high-dimensional, directly using the entire matrix as input would result in the curse of dimensionality. Consequently, the condition embedding module utilizes an attention mechanism to convert the high-dimensional single-cell data matrix into a lower-dimensional representation. This reduces the data to a low-dimensional, high-expression latent representation, which is then used as a conditional mechanism in subsequent diffusion model training.

For the input of Condition Embedding, the high-dimensional input matrix X_{sc} is processed using Flash-attention to compute a lower-dimensional representation X_ψ as output:

$$Q = X_{sc}W^Q, K = X_{sc}W^K, V = X_{sc}W^V, \quad (1)$$

$$X_\psi = \text{softmax}\left(\frac{Q\Phi_K(K)^T}{\sqrt{d_k}}\right)\Phi_V(V)$$

Where:

- W^Q , W^K , and W^V are projection matrices that transform X into queries Q , keys K , and values V , respectively.
- Φ_K and Φ_V are the dimensionality reduction functions applied to K and V , resulting in lower-dimensional.

- d_k is the dimension of K after projection, used to scale the softmax computation.
- The softmax function is applied over each row, normalizing the dot product scores into a probability distribution used to compute the weighted sum of values $\Phi_V(V)$.

Diffusion with Transformer in SpaDiT

The backbone network of our proposed SpaDiT is Diffusion Transformers (DiTs), a new architecture for diffusion models. For the backbone network model, we refer to previous work [36] and make modifications based on the challenges we encounter. Our backbone model has two types of input: x_ϕ , representing latent embedding, and x_ψ , representing condition embedding. We initialize each residual block in the backbone network as an identity function and incorporate the condition embedding into the backbone. At each layer, we also perform scaling regression on all residual connections within the backbone, facilitating rapid model convergence.

After the final DiT block, the gene expression token sequence needs to be decoded into output noise prediction and output diagonal covariance prediction. The shapes of both outputs are identical to the input in the original space, and a standard linear decoder is employed to achieve this. Finally,

the decoded tokens are rearranged to match the layout of the original expression, yielding the predicted noise and covariance.

Training phase in SpaDiT

Here in, SpaDiT works with two types of input data: the spatial transcriptomics data $X_{st} = \{x_{st}^i\}_i^n \in \mathbb{R}^{n \times p}$ and scRNA-seq data $X_{sc} = \{x_{sc}^j\}_j^m \in \mathbb{R}^{m \times q}$. Among them, n and p respectively represent the number of genes and the number of spots in spatial transcriptomics data, and m and q respectively represent the number of genes and the number of cells in scRNA-seq data.

The training phase of SpaDiT is shown in the Figure 1 (A). We first mask the genes of the original spatial transcriptomics data according to a certain proportion, where the mask is divided into two parts: the part with an expression value of zero and the part with an expression value that is not zero. The input tensor of the training phase is defined as follows:

$$x_0 = \hat{x}_{st}^i \oplus \hat{x}_{sc}^i \quad (2)$$

where \hat{x}_{st}^i and \hat{x}_{sc}^i are projection of x_{st}^i and x_{sc}^i by a simple feed-forward network.

In the realm of DDPMs [23, 37], consider the task of learning a model distribution $p_\theta(\mathbf{x}_0)$ that closely approximates a given data distribution $q(\mathbf{x}_0)$. Suppose we have a sequence of latent variables \mathbf{x}_t for $t = 1, \dots, T$, existing within the same sample space as \mathbf{x}_0 , which is denoted as \mathcal{X} . DDPMs are latent variable models that are composed of two primary processes: the forward process and the reverse process. The forward process is defined by a Markov chain, as follows:

$$q(\mathbf{x}_{1:T} | \mathbf{x}_0) := \prod_{t=1}^T q(\mathbf{x}_t | \mathbf{x}_{t-1}), \quad (3)$$

where $q(\mathbf{x}_t | \mathbf{x}_{t-1}) := \mathcal{N}(\sqrt{1 - \beta_t} \mathbf{x}_{t-1}, \beta_t \mathbf{I})$, and the variable β_t is a small positive constant indicative of a noise level. The sampling of x_t can be described by the closed-form expression $q(x_t | x_0) = \mathcal{N}(x_t; \sqrt{\alpha_t} x_0, (1 - \alpha_t) \mathbf{I})$, where $\hat{\alpha}_t := 1 - \beta_t$ and α_t is the cumulative product $\alpha_t := \prod_{i=1}^t \hat{\alpha}_i$. Consequently, x_t is given by the equation $x_t = \sqrt{\alpha_t} x_0 + (1 - \alpha_t) \epsilon$, with $\epsilon \sim \mathcal{N}(0, \mathbf{I})$. In contrast, the reverse process aims to denoise x_t to retrieve x_0 , a process which is characterized by the ensuing Markov chain:

$$\begin{aligned} p_\theta(\mathbf{x}_{0:T}) &:= p(\mathbf{x}_T) \prod_{t=1}^T p_\theta(\mathbf{x}_{t-1} | \mathbf{x}_t), \quad \mathbf{x}_T \sim \mathcal{N}(0, \mathbf{I}), \\ p_\theta(\mathbf{x}_{t-1} | \mathbf{x}_t) &:= \mathcal{N}(\mathbf{x}_{t-1}; \mu_\theta(\mathbf{x}_t, t), \sigma_\theta^2(\mathbf{x}_t, t) \mathbf{I}), \\ \mu_\theta(\mathbf{x}_t, t) &= \frac{1}{\alpha_t} \left(\mathbf{x}_t - \frac{\beta_t}{\sqrt{1 - \alpha_t}} \epsilon_\theta(\mathbf{x}_t, t) \right), \\ \sigma_\theta(\mathbf{x}_t, t) &= \beta_t^{1/2} \end{aligned} \quad (4)$$

where $\epsilon_\theta(\mathbf{x}_t, t)$ is a trainable denoising function and

$$\beta_t = \begin{cases} \frac{1 - \hat{\alpha}_{t-1}}{1 - \hat{\alpha}_t} \beta_1, & \text{for } t > 1, \\ \beta_1, & \text{for } t = 1. \end{cases} \quad (5)$$

SpaDiT aims to help models understand and estimate the expression of missing genes in ST data by utilizing scRNA-seq data as prior information, thereby enabling the model to better predict gene expression from ST data. We represent the data of the condition as $x_0^c = x_\psi$. Therefore, our goal is to estimate the posterior $p((E_{n,1} - m_1) \odot ((E_{n,1} - m_2) \odot x_0) | x_0^c)$, where $E_{n,1}$

is an all-1 matrix $n \times 1$ with dimension, $m_1, m_2 \in \{0, 1\}^{n \times 1}$ is an element-wise indicator, representing the zero and non-zero parts of the mask respectively.

We also denote predicted genes as x_t^* , where t is the time step. Therefore, the goal of our SpaDiT conditional mechanism is to estimate the probability:

$$p_\theta(x_{t-1}^* | x_t^*, x_0^c). \quad (6)$$

In order to better use the scRNA-seq data as a priori conditions for the diffusion model to perform predicting gene expression, we transform the Equation 3 and Equation 4 into:

$$\begin{aligned} p_\theta(x_{0:T}^* | x_0^c) &:= p(x_T^*) \prod_{t=1}^T p_\theta(x_{t-1}^* | x_t^*, x_0^c), \quad x_T^* \sim \mathcal{N}(0, \mathbf{I}), \\ p_\theta(x_{t-1}^* | x_t^*, x_0^c) &:= \mathcal{N}(x_{t-1}^*; \mu_\theta(x_t^*, t | x_0^c), \sigma_\theta(x_t^*, t | x_0^c) \mathbf{I}). \end{aligned} \quad (7)$$

We can optimize the Equation 7 parameters by minimizing the variational lower bound:

$$\mathbb{E}_q[-\log p_\theta(x_0 | x_0^c)] \leq \mathbb{E}_q \left[-\log \frac{p_\theta(x_{0:T} | x_0^c)}{q(x_{1:T} | x_0)} \right]. \quad (8)$$

Also we can get a simplified training objective:

$$\mathbb{E}_{x_0 \sim q(\mathbf{x}_0), \epsilon \sim \mathcal{N}(0, \mathbf{I}), t} \| (\epsilon - \epsilon_\theta(\mathbf{x}_t^*, t | x_0^c)) \|_2^2. \quad (9)$$

We provide the training procedure of SpaDiT in Algorithm 1.

Algorithm 1 Training of SpaDiT

- 1: **Input:** ST data $X_{st} = \{x_{st}^i\}_i^n \in \mathbb{R}^{n \times p}$, SC data $X_{sc} = \{x_{sc}^j\}_j^m \in \mathbb{R}^{m \times q}$, Number of iterations N_{iter} , $\{\alpha_t\}_{t=1}^T$, T
- 2: **Output:** Trained denoising function ϵ_θ
- 3: **for** $i = 1$ to N_{iter} **do**
- 4: $x_i \sim X_{st}$, $x_j \sim X_{sc}$
- 5: $x_0 = \Phi(x_i, x_j)$, $x_0^c = \psi(X_{sc})$, where $[i, j] \in (X_{st} \cap X_{sc})$
- 6: $t \sim \text{Uniform}(\{1, \dots, T\})$
- 7: $\epsilon \sim \mathcal{N}(0, \mathbf{I})$
- 8: Take gradient step on

$$\nabla_\theta \| (\epsilon - \epsilon_\theta(\sqrt{\alpha_t} x_0^* + \sqrt{1 - \alpha_t} \epsilon, t | x_0^c)) \|_2^2$$

9: **end for**

Inference phase in SpaDiT

We focus on improving the conditional diffusion model characterized by the inverse process described in Equation 7. Our goal is to accurately model the conditional distribution $p(x_{t-1}^* | x_t^*, x_0^c)$ without resorting to approximations. To achieve this, we adapt the parameterization of DDPM from Equation 4 for the conditional setting. We introduce a conditional denoising function $\epsilon_\theta : (\mathcal{X}^* \times \mathbb{R} | \mathcal{X}^c) \rightarrow \mathcal{X}^*$ accepts conditional observation value x_0^c as input parameter. On this basis, we use ϵ_θ for parameterization, as follows:

$$\begin{aligned} \mu_\theta(x_t^*, t | x_0^c) &= \mu(x_t^*, t, s_\theta(x_t^*, t | x_0^c)), \\ \sigma_\theta(x_t^*, t | x_0^c) &= \sigma(x_t^*, t), \end{aligned} \quad (10)$$

where μ and σ are defined in Equation 4. Utilizing the function ϵ_θ and the data x_0 , we can simulate samples of x_0^* by employing the reverse process outlined in Equation 7. We provide the inference procedure of SpaDiT in Algorithm 2.

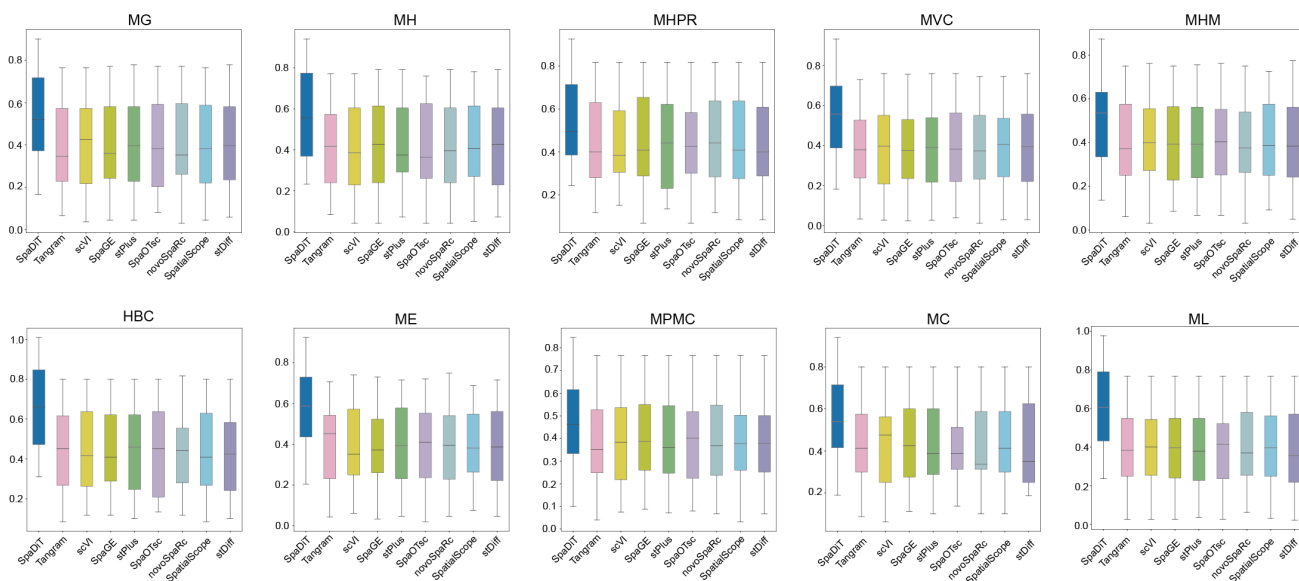


Fig. 2. Performance evaluation is based on the comprehensive metric of Accuracy Score (AS) on ten real paired ST and scRNA-seq datasets. Accuracy Score (AS) is a comprehensive indicator for evaluating model performance. The definition can be found in [subsection 2.3](#). The central line represents the median, the box depicts the interquartile range, whiskers extend to 1.5 times the interquartile range, and dots represent the AS of individual datasets.

Algorithm 2 Inference of SpaDiT

- 1: **Input:** Gaussian Noise $\mathcal{N}(0, I)$, SC data $X_{sc} = \{x_{sc}^i\}_i^m \in \mathbb{R}^{m \times q}$
 - 2: **Output:** Predicted gene expression x_0
 - 3: **for** $t = T$ to 1 **do**
 - 4: $x_t^c = \psi(X_{sc})$
 - 5: Sample $x_t, \epsilon_t \sim \mathcal{N}(0, I)$
 - 6: $x_t = \Phi(x_t, x_{sc}^i)$, where $[i] \in (X_{st} \cap X_{sc})$
 - 7: $x_{t-1} \leftarrow \frac{1}{\sqrt{\alpha_t}} \left(x_t - \frac{1-\alpha_t}{\sqrt{1-\alpha_t}} \epsilon_\theta(x_t, t|x_t^c) \right) + \sqrt{\beta_t} \epsilon_t$
 - 8: $t \leftarrow t - 1$
 - 9: **end for**
-

Evaluation metrics

To evaluate the performance of SpaDiT and other baseline methods, we use five evaluation indicators: Pearson Correlation Coefficient (PCC), Structural Similarity Index Measure (SSIM), Root Mean Square Error (RMSE), Jensen-Shannon Divergence (JS) and Accuracy Score (AS) to evaluate the gene prediction performance of different methods on ten datasets. The specific definition of the evaluation metrics can be found in [Supplementary Materials](#).

Baselines

We compared the performance of SpaDiT to eight baseline methods, with data processing procedures (e.g., normalization and scaling) consistent for each method. The specific baselines are as follows:

- Tangram [14]: It is a method that can map any type of sc/snRNA-seq data, including multimodal data such as those from SHARE-seq, which can be used to reveal spatial patterns of chromatin accessibility. We refer to the guide on the Tangram GitHub repository: <https://github.com/broadinstitute/Tangram>.
- scVI [15]: It is a scalable framework for probabilistic representation and analysis of single-cell gene expression.

We refer to the guide on the scVI GitHub repository: <https://github.com/YosefLab/scVI>.

- SpaGE [16]: It is a method that integrates spatial and scRNA-seq datasets to predict whole-transcriptome expressions in their spatial configuration. We refer to the guide on the SpaGE GitHub repository: <https://github.com/tabelaal/SpaGE>.
- stPlus [17]: It is a reference-based method that leverages information in scRNA-seq data to enhance spatial transcriptomics. We refer to the guide on the stPlus GitHub repository: <https://github.com/xy-chen16/stPlus>.
- SpaOTsc [18]: It is a method that relies on structured optimal transfer to recover the spatial properties of scRNA-seq data by exploiting spatial measurements of a relatively small number of genes. We refer to the guide on the SpaOTsc GitHub repository: <https://github.com/zcang/SpaOTsc>.
- novoSpaRc [19]: It is a method that reconstructs tissue based on this hypothesis and optionally improves the reconstruction by including a reference map of marker genes. We refer to the guide on the SpaOTsc GitHub repository: <https://github.com/rajewsky-lab/novosparc>.
- SpatialScope [20]: It is a method to integrate scRNA-seq reference data and ST data using deep generative models. We refer to the guide on the SpatialScope GitHub repository: <https://github.com/YangLabHKUST/SpatialScope>.
- stDiff [21]: It is a method that capturing gene expression abundance relationships in scRNA-seq data through two Markov processes. We refer to the guide on the stDiff GitHub repository: <https://github.com/fdu-wangfeilab/stDiff>

Table 2. Comparison with baseline methods on the ten paired scRNA-seq and ST datasets.

PCC↑	MG	MH	MHPR	MVC	MHM	HBC	ME	MPMC	MC	ML
Tangram [14]	0.458±0.203	0.523±0.116	0.683±0.012	0.623±0.117	0.536±0.053	0.703±0.142	0.503±0.025	0.727±0.026	0.745±0.003	0.714±0.056
scVI [15]	0.476±0.157	0.446±0.157	0.691±0.143	0.594±0.023	0.511±0.117	0.656±0.005	0.496±0.007	0.716±0.014	0.736±0.015	0.637±0.001
SpaGE [16]	0.526±0.114	0.438±0.163	0.653±0.063	0.603±0.107	0.545±0.226	0.639±0.025	0.512±0.013	0.753±0.066	0.769±0.011	0.653±0.007
stPlus [17]	0.503±0.233	0.401±0.037	0.483±0.231	0.574±0.059	0.476±0.007	0.597±0.111	0.526±0.026	0.689±0.007	0.701±0.099	0.699±0.014
SpaOTsc [18]	0.522±0.014	0.485±0.107	0.657±0.002	0.629±0.147	0.496±0.018	0.587±0.107	0.547±0.006	0.734±0.201	0.738±0.064	0.723±0.005
novoSpaRc [19]	0.563±0.158	0.567±0.252	0.613±0.146	0.656±0.037	0.515±0.003	0.647±0.122	0.569±0.013	0.756±0.015	0.756±0.015	0.766±0.056
SpatialScope [20]	0.612±0.143	0.582±0.183	0.637±0.031	0.683±0.114	0.547±0.103	0.733±0.183	0.563±0.056	0.769±0.022	0.776±0.006	0.803±0.014
stDiff [21]	0.482±0.021	0.527±0.013	0.621±0.007	0.601±0.043	0.471±0.009	0.544±0.021	0.553±0.014	0.629±0.011	0.604±0.019	0.736±0.099
SpaDiT (Ours)	0.657±0.035	0.621±0.099	0.770 ±0.043	0.725±0.106	0.573±0.083	0.772±0.057	0.590±0.146	0.808±0.043	0.812±0.039	0.784±0.096
SSIM↑	MG	MH	MHPR	MVC	MHM	HBC	ME	MPMC	MC	ML
Tangram [14]	0.355±0.114	0.541±0.203	0.681±0.025	0.653±0.115	0.388±0.109	0.656±0.007	0.521±0.047	0.889±0.043	0.789±0.004	0.689±0.005
scVI [15]	0.487±0.155	0.422±0.128	0.647±0.121	0.564±0.025	0.374±0.115	0.617±0.028	0.587±0.013	0.674±0.012	0.736±0.006	0.694±0.014
SpaGE [16]	0.503±0.003	0.403±0.158	0.631±0.011	0.611±0.004	0.401±0.006	0.588±0.189	0.513±0.064	0.653±0.011	0.667±0.055	0.703±0.023
stPlus [17]	0.533±0.114	0.367±0.127	0.657±0.176	0.656±0.007	0.426±0.013	0.638±0.221	0.479±0.023	0.627±0.103	0.693±0.011	0.736±0.014
SpaOTsc [18]	0.547±0.126	0.503±0.013	0.701±0.026	0.637±0.021	0.484±0.170	0.626±0.118	0.601±0.188	0.663±0.114	0.718±0.004	0.688±0.007
novoSpaRc [19]	0.587±0.028	0.537±0.026	0.713±0.123	0.631±0.018	0.477±0.201	0.633±0.107	0.622±0.023	0.726±0.055	0.726±0.006	0.705±0.006
SpatialScope [20]	0.612±0.016	0.588±0.014	0.731±0.054	0.674±0.026	0.512±0.122	0.659±0.055	0.701±0.022	0.826±0.014	0.753±0.014	0.714±0.004
stDiff [21]	0.463±0.017	0.548±0.118	0.673±0.013	0.576±0.007	0.462±0.017	0.514±0.012	0.563±0.017	0.598±0.019	0.701±0.023	0.688±0.017
SpaDiT (Ours)	0.632±0.037	0.574±0.125	0.738±0.044	0.689±0.114	0.495±0.175	0.717±0.111	0.688±0.144	0.781±0.050	0.787±0.042	0.751±0.107
RMSE↓	MG	MH	MHPR	MVC	MHM	HBC	ME	MPMC	MC	ML
Tangram [14]	1.263±0.053	1.412±0.018	1.263±0.012	1.587±0.041	1.237±0.005	1.542±0.003	1.633±0.004	1.324±0.048	1.216±0.184	1.346±0.015
scVI [15]	1.155±0.012	1.363±0.026	1.374±0.026	1.327±0.106	1.213±0.103	1.378±0.005	1.581±0.013	1.207±0.034	1.179±0.067	1.411±0.056
SpaGE [16]	1.187±0.025	1.433±0.037	1.287±0.029	1.354±0.047	1.347±0.025	1.413±0.101	1.553±0.024	1.137±0.011	1.213±0.005	1.233±0.008
stPlus [17]	1.254±0.003	1.367±0.045	1.384±0.121	1.289±0.022	1.156±0.014	1.331±0.077	1.496±0.033	1.656±0.007	1.154±0.024	1.303±0.014
SpaOTsc [18]	1.433±0.058	1.213±0.058	1.203±0.027	1.253±0.007	1.227±0.058	1.203±0.114	1.403±0.004	1.227±0.026	1.016±0.007	1.263±0.005
novoSpaRc [19]	1.275±0.143	1.526±0.213	1.252±0.011	1.206±0.014	1.412±0.117	1.198±0.007	1.556±0.021	1.334±0.015	0.967±0.153	1.523±0.007
SpatialScope [20]	1.019±0.022	1.288±0.258	1.201±0.003	1.009±0.007	1.217±0.005	1.102±0.005	1.483±0.007	1.104±0.056	0.863±0.004	1.343±0.014
stDiff [21]	1.326±0.019	1.325±0.022	1.081±0.013	1.219±0.066	1.312±0.007	1.217±0.023	1.561±0.023	1.326±0.016	1.224±0.003	1.223±0.009
SpaDiT (Ours)	0.877±0.049	1.103±0.015	1.184±0.058	1.116±0.038	1.125±0.060	0.992±0.045	1.376±0.118	1.089±0.038	1.004±0.037	1.121±0.047
JS↓	MG	MH	MHPR	MVC	MHM	HBC	ME	MPMC	MC	ML
Tangram [14]	0.477±0.057	0.254±0.003	0.458±0.033	0.343±0.007	0.502±0.056	0.397±0.105	0.803±0.026	0.403±0.056	0.547±0.005	0.347±0.014
scVI [15]	0.426±0.088	0.324±0.147	0.496±0.011	0.403±0.001	0.537±0.113	0.427±0.089	0.749±0.015	0.423±0.115	0.601±0.014	0.363±0.047
SpaGE [16]	0.437±0.054	0.272±0.023	0.511±0.007	0.387±0.114	0.528±0.007	0.415±0.026	0.882±0.003	0.374±0.004	0.617±0.006	0.403±0.011
stPlus [17]	0.481±0.146	0.288±0.057	0.503±0.014	0.399±0.005	0.488±0.125	0.439±0.005	0.814±0.036	0.393±0.005	0.576±0.004	0.423±0.016
SpaOTsc [18]	0.513±0.126	0.334±0.058	0.411±0.022	0.403±0.147	0.503±0.111	0.411±0.015	0.792±0.007	0.417±0.011	0.463±0.026	0.311±0.007
novoSpaRc [19]	0.488±0.003	0.401±0.017	0.389±0.005	0.412±0.003	0.496±0.015	0.429±0.085	0.683±0.015	0.401±0.005	0.431±0.005	0.401±0.006
SpatialScope [20]	0.403±0.002	0.263±0.174	0.366±0.007	0.389±0.008	0.487±0.026	0.455±0.002	0.622±0.150	0.389±0.107	0.407±0.014	0.355±0.014
stDiff [21]	0.467±0.001	0.412±0.015	0.387±0.021	0.461±0.011	0.467±0.021	0.456±0.011	0.663±0.017	0.436±0.022	0.432±0.063	0.396±0.007
SpaDiT (Ours)	0.346±0.012	0.246±0.005	0.337±0.010	0.369±0.029	0.463±0.116	0.381±0.061	0.549±0.134	0.356±0.012	0.371±0.013	0.421±0.064

Results

SpaDiT improves prediction accuracy of spatial gene expression

To rigorously assess the SpaDiT method’s capabilities in predicting gene expression, we conducted a comparative analysis with eight other widely recognized methods in the field. We used four key performance metrics, as outlined in subsection 2.3, to systematically evaluate both SpaDiT and the comparator baseline methods. The evaluation focused on computing the mean and variance of these metrics across all genes within each dataset. The results are depicted in Table 2.

Our findings indicate that SpaDiT consistently achieves state-of-the-art (SOTA) performance in all four metrics across the ten examined datasets. However, it is important to note that in a few cases, SpaDiT slightly lags behind some established methods in one particular metric. This deviation provides critical insights into scenarios where SpaDiT might be further optimized.

In addition to these traditional metrics, we introduced an advanced scoring system, referred to as AS metrics, to further evaluate SpaDiT’s performance. The results, illustrated in Figure 2, confirm that SpaDiT not only meets but often exceeds the performance benchmarks set by the baseline methods across all ten spatial transcriptomics (ST) datasets. The inclusion of AS metrics provides a more nuanced understanding of SpaDiT’s predictive prowess, underscoring its robustness and effectiveness in diverse experimental conditions. This comprehensive approach solidifies SpaDiT’s position as a leading method in gene expression prediction, highlighting its

potential to significantly enhance the accuracy and reliability of spatial transcriptomics analyses.

SpaDiT enhances the similarity of predicted gene expression in high-dimensional space

To fully demonstrate the superior ability of the SpaDiT method in gene expression prediction, especially its advantages in maintaining the global and local structural characteristics of gene expression data, we used UMAP technology for visualization analysis for conducting in-depth comparisons with other benchmark methods.

As shown in the Figure 3, we conducted an analysis of ten different datasets. The results clearly show that the prediction results of the SpaDiT method (in orange) closely resemble the real gene expression data (in blue), with minimal perceptible deviation. This is in sharp contrast to the prediction results generated by several other methods, such as Tangram, scVI, SpaGE, stPlus, SpaOTsc, novoSpaRc, SpatialScope, and stDiff. Although the prediction results of these methods have their own focuses, compared with SpaDiT, they all fail to accurately capture the structural characteristics of real gene data and exhibit significant deviations. In addition, the UMAP analysis further underscores SpaDiT’s superiority in maintaining data integrity, enabling it to accurately simulate complex biological information.

SpaDiT preserves the similarity between genes

To fully demonstrate the accuracy of the SpaDiT method in predicting gene expression, we employed hierarchical clustering

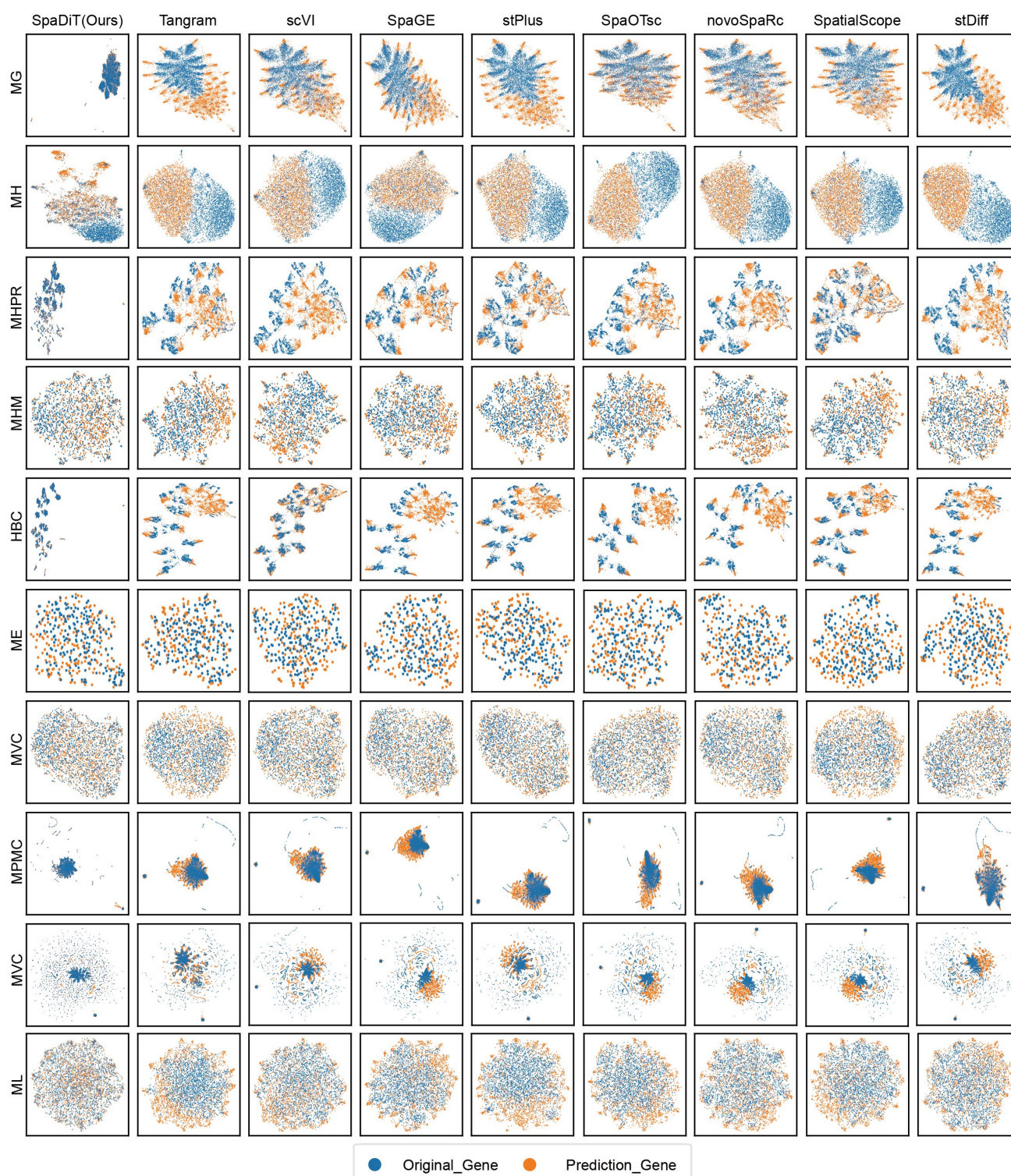


Fig. 3. UMAP plots illustrating gene predicted by SpaDiT, Tangram, scVI, SpaGE, stPlus, SpaOTsc, novoSpaRc, SpatialScope and stDiff. The closer the two scatter points are, the better the prediction effect is. The scatter points predicted by SpaDiT and the real scatter points almost overlap, indicating that the genes predicted by SpaDiT are closer to the real genes.

to visualize the similarity between the predicted genes and the true gene labels, and compared the results with those from other benchmark methods.

First, we calculated the Euclidean distance between each pair of genes in the gene expression matrix predicted by each method to reflect the similarity of the expression patterns of two genes: the smaller the distance, the higher the similarity. After

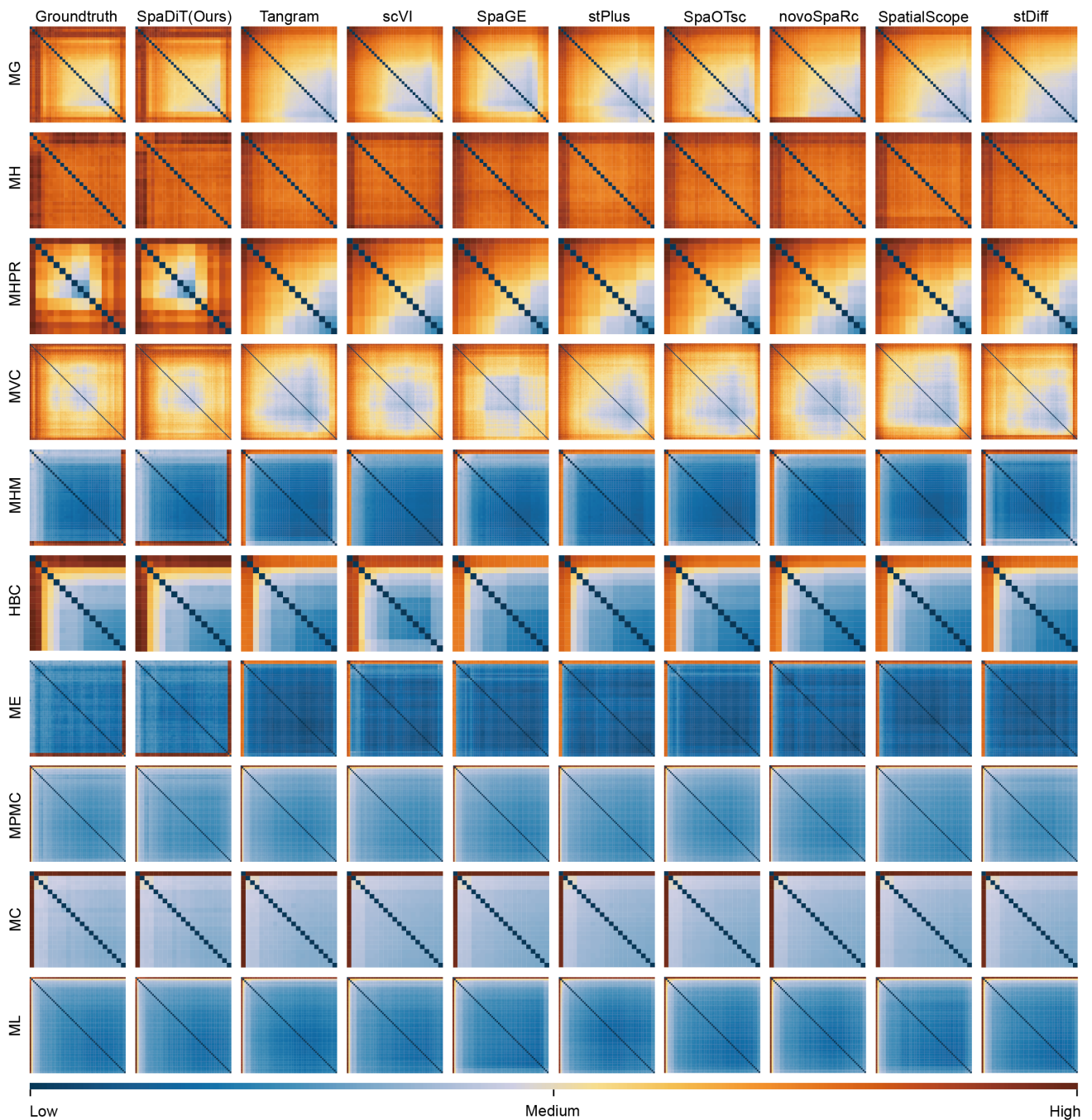


Fig. 4. Visualization of the prediction performance of various baseline methods. The first column of the figure shows the results after clustering the true labels. The closer the predicted results of each method are to the true labels, the better the effect. The clustering effect of SpaDiT is closest to the true labels.

calculating the distance of all gene pairs, we used hierarchical clustering to sort these genes to ensure that the genes within the cluster show the greatest similarity. With this sorting, we can reorganize the rows and columns of the distance matrix so that similar genes are adjacent to each other in the heat map.

As shown in the [Figure 4](#), the first column of the figure visualizes the true gene labels after clustering. The closer the predicted gene heat map is to the true labels, the higher the prediction accuracy of the method. As evident from the figure, the prediction results of the SpaDiT method are very close to

the true labels, demonstrating its high accuracy in predicting gene expression.

SpaDiT accurately predicts ST Spatial Patterns

In addition to quantitatively evaluating the gene expression similarity between the true genes of ST and the genes predicted by ST, we also visually demonstrate the consistency of spatial patterns in [Figure 5](#).

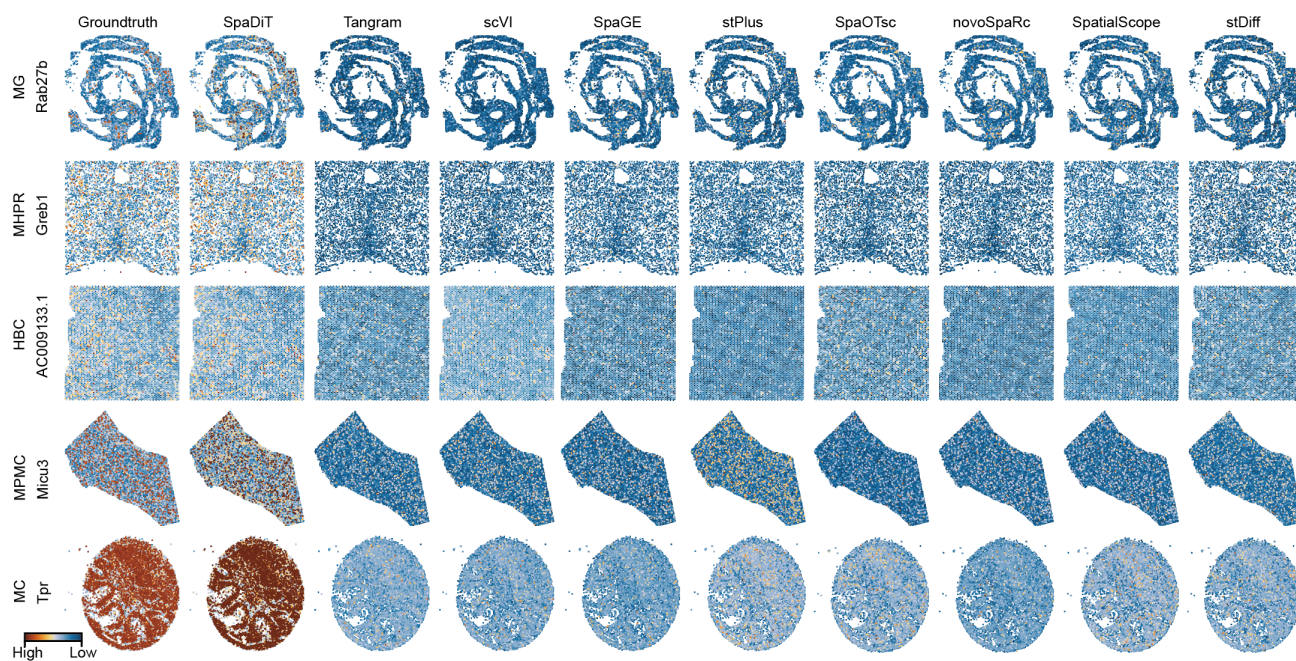


Fig. 5. Predicted expression abundance of genes with known spatial patterns in four datasets. Each column corresponds to a gene with a clear spatial pattern. The first column represents the spatial pattern genes with true labels. Subsequent columns show the corresponding predicted expression patterns obtained by using SpaDiT, Tangram, scVI, SpaGE, stPlus, SpaOTsc, novoSpaRc, SpatialScope, and stDiff.

Due to limited space, we selected five datasets with clear spatial patterns: MG, MHPR, HBC, MPMC, and MC to illustrate the consistency of the spatial patterns between the genes predicted by the methods and the true labels. We display the predicted genes with the highest Pearson correlation coefficient (PCC) values in the datasets. The other five datasets not shown can be found in the [Supplementary Materials](#).

As illustrated in [Figure 5](#), in the MG dataset, SpaDiT restores the overall spatial pattern more accurately, followed by stDiff and stPlus, while the other methods show less obvious spatial contours in the upper right part. In the MHPR dataset, SpaDiT provides more accurate predictions in the middle part, while the high expression area and low expression area of other methods appear somewhat chaotic. In the HBC and MPMC datasets, all methods predict relatively accurate spatial patterns, but SpaDiT is the method with expression value predictions closest to the true labels. In the MC dataset, SpaDiT has a clear spatial recognition contour for the lower half, which is closest to the actual situation, while other methods are more blurred at the boundary.

Robustness evaluation of SpaDiT across various sampling rates

In our study, the sparsity of the ten dataset pairs varies. Most of the datasets are highly sparse spatial transcriptomic data, except for the MH dataset, which has a sparsity of 6.7%. To test the ability of SpaDiT to resist data sparsity, we downsampled the expression matrix of MH’s spatial transcriptomics data to simulate different high-sparse data. To quantify the stability of the SpaDiT and its ability to resist data sparsity, we counted the percentage of genes with a prediction accuracy (PCC) greater than 0.5 in both the original data and the downsampled data, defined as the Robustness Score (RS). As shown in the [Figure 6](#), the red points represent genes with a PCC value

greater than 0.5, and the gray points represent genes with a PCC value less than 0.5. We tested different downsampling rates: 0.1, 0.3, 0.5, and 0.7, and found that the stability scores of all methods decreased with the increase of data sparsity, while the stability score of SpaDiT was always higher than that of other baseline methods. In addition, we compared the changing trends of model performance under different sampling rates and different sparsity levels on ten datasets. For detailed results on other datasets, please refer to the [Supplementary Materials](#).

Ablation studies: The impact of different modules of SpaDiT on model performance

As mentioned above, Condition Embedding and Backbone network in SpaDiT are the key parts of our proposed method. In order to verify the importance of these two parts, we conducted ablation experiments in this section.

For the backbone network part ([Figure 1](#)), we used three different network backbones and used AS as the evaluation indicator. As shown in the [Table 3](#), we compared three different network architectures: U-Net, Mamba, and Transformer. It is worth noting that the model using Transformer as the network backbone has the best performance, which further proves the importance of Transformer and verifies the superiority of SpaDiT.

In our proposed, SpaDiT, the main innovation involves using spatial transcriptomics (ST) and single-cell (SC) common genes to concatenate by gene in latent embedding. We use the known part (concatenated SC gene) to infer the gene expression of the unknown part (ST gene to be predicted). This approach enables the model to learn the similarity between different spots and cells across genes. Additionally, the Condition module utilizes the overall SC data as the prior condition to guide the model’s generation process. To verify the effectiveness of the

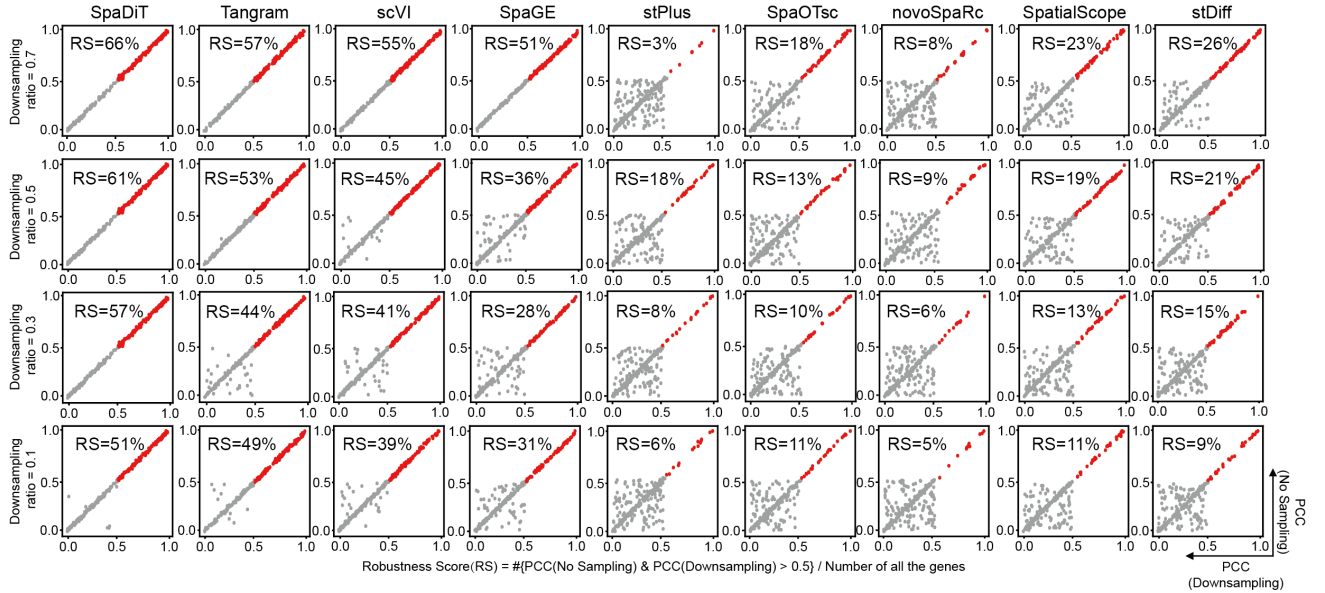


Fig. 6. Robustness of prediction accuracy for original data and data with different downsampling rates for the MH dataset. PCC of the spatial distribution of transcripts predicted from the original data and the MH dataset at different downsampling ratios. The PCC values of red transcripts are greater than 0.5 for both the original data and the downsampled data. The proportion of red transcripts in all transcripts is defined as the “robustness score” (RS).

Table 3. Result of different network backbone.

	MG	MH	MHPR	MVC	MHM
Backbone w/Unet	0.454±0.011	0.453±0.011	0.477±0.013	0.482±0.011	0.466±0.011
Backbone w/Mamba	0.477±0.008	0.471±0.026	0.475±0.014	0.474±0.011	0.461±0.102
Backbone w/Transformer	0.514±0.032	0.553±0.057	0.506±0.038	0.572±0.033	0.553±0.037
	HBC	ME	MPMC	MC	ML
Backbone w/Unet	0.478±0.012	0.470±0.010	0.458±0.013	0.470±0.010	0.487±0.013
Backbone w/Mamba	0.462±0.086	0.489±0.051	0.421±0.022	0.478±0.015	0.488±0.021
Backbone w/Transformer	0.613±0.024	0.589±0.060	0.488±0.033	0.564±0.026	0.619±0.024

proposed method, we conducted ablation experiments on these two modules separately.

The specific experimental results are shown in Table 4. First, for the Condition module (ψ), to verify the effectiveness of the Attention mechanism, we replaced Attention with a simple MLP (Part: w/o Flash-Attention). We found that the performance of the model dropped significantly across ten datasets. Further, to verify the effectiveness of the Condition module (ψ) (Part: w/o Condition ψ), we replaced the output of the entire part with a vector of all zeros. We observed that compared to replacing Attention, the performance of the model further declined. Additionally, to verify the effectiveness of the

overall SC data as a priori conditions (Part: w/ Common Gene in ψ), we replaced the overall SC data with SC that only retained the common genes. We found that the performance also declined compared to the overall SC. Finally, to verify the effectiveness of the splicing of the common genes (Part: w/o Concat in ϕ), we removed this part and found that the performance significantly declined. Therefore, we conclude that the method we proposed is highly effective. In addition, we also tried using Condition modules with different Condition methods. For details, please refer to the [Supplementary Materials](#).

Table 4. Ablation study of Condition Embedding module and Latent Embedding module.

	MG	MH	MHPR	MVC	MHM
SpaDiT(Ours)	0.514±0.032	0.553±0.057	0.506±0.038	0.572±0.033	0.553±0.037
w/o Flash-Attention	0.439±0.092	0.485±0.027	0.431±0.028	0.429±0.013	0.415±0.017
w/o Condition ψ	0.383±0.094	0.336±0.115	0.404±0.161	0.394±0.066	0.318±0.013
w/ Common Gene in ψ	0.483±0.126	0.503±0.008	0.437±0.125	0.533±0.161	0.489±0.088
w/o Concat in ϕ	0.462±0.093	0.501±0.140	0.432±0.020	0.489±0.076	0.485±0.042
	HBC	ME	MPMC	MC	ML
SpaDiT(Ours)	0.613±0.024	0.589±0.060	0.488±0.033	0.564±0.026	0.619±0.024
w/o Flash-Attention	0.431±0.034	0.422±0.021	0.425±0.013	0.438±0.019	0.459±0.033
w/o Condition module: ψ	0.407±0.053	0.376±0.169	0.401±0.050	0.417±0.108	0.423±0.022
w/ Common Gene in ψ	0.537±0.032	0.426±0.142	0.411±0.083	0.503±0.050	0.526±0.062
w/o Concat in ϕ	0.407±0.128	0.512±0.161	0.311±0.106	0.489±0.074	0.503±0.114

Discussion

In this paper, we present SpaDiT, a novel approach to predict unmeasured genes in spatial transcriptomics (ST) data. Methodologically, SpaDiT is significantly different from existing ensemble techniques. While traditional approaches primarily enhance ST data by aligning ST data to similar cells within a reference scRNA-seq dataset, SpaDiT employs a diffusion-based generative model that utilizes the inherent relationships within the gene expression data. This approach enables it to precisely model and generate spatial gene expression patterns.

SpaDiT, as a conditional diffusion model, employs noise addition and denoising stages to learn complex relationships from scRNA-seq data. In the inference stage, SpaDiT incorporates raw ST data during the denoising process, resulting in accurate predictions of spatial gene expression. The application of diffusion models in genomics, especially transcriptomics, is relatively new, marking this as a largely unexplored area. We assessed SpaDiT using ten ST datasets, employing multiple metrics to evaluate performance, gene spatial structure, and gene similarity. The results show that SpaDiT not only maintains the intricate topology inherent in cell layout but also excels in accurately aligning predicted gene expression with actual data, demonstrating its robustness and accuracy in reproducing spatial patterns. These features highlight the utility of SpaDiT in enhancing the resolution and richness of ST data analysis.

Future research may combine SpaDiT's diffusion-based approach with traditional similarity-based methods to enhance the accuracy of ST data predictions. These advances may significantly improve the analysis and interpretation of ST data, potentially setting new standards in the field. It is important to acknowledge the potential limitations. For example, when ST data lack sufficient markers to accurately identify cell types, SpaDiT's efficacy may be diminished, similar to other methods. This is due to the reliance on existing gene expression signals to guide the prediction process, potentially resulting in inaccuracies if the initial data are too sparse or ambiguous. This underscores the need for improvements in handling datasets with limited information, ensuring that SpaDiT can adapt to various levels of data completeness and quality.

Key Points

- In this study, we propose SpaDiT, a deep learning method that utilizes a conditional diffusion generative model to synthesize scRNA-seq data and ST data to predict undetected genes.
- We utilize scRNA-seq as a prior condition and integrate it into the diffusion model through the attention mechanism to guide the model in learning the relationship between ST and scRNA-seq. At the same time, the common genes in ST and scRNA-seq are concatenated as the "token" input of the model, so that SpaDiT can learn multi-scale feature information and more accurately predict unknown genes.
- Our method was compared with competing methods on ten real ST and scRNA-seq datasets. The results show that, compared with the most

advanced methods, our method demonstrates significant improvements in all five evaluation metrics in predicting gene expression. In addition, the genes predicted by our proposed SpaDiT effectively maintain high-dimensional similarity with the real labels, clearly restoring the spatial patterns between genes and the similarities between genes.

Acknowledgments

The work was supported in part by the National Natural Science Foundation of China (62262069), in part by the Yunnan Fundamental Research Project (202301BF070001-019) and the Yunnan Talent Development Program - Youth Talent Project.

References

1. Angela R Wu, Norma F Neff, et al. Quantitative assessment of single-cell rna-sequencing methods. *Nature Methods*, 11(1):41–46, 2014.
2. Sophia K Longo, Margaret G Guo, et al. Integrating single-cell and spatial transcriptomics to elucidate intercellular tissue dynamics. *Nature Reviews Genetics*, 22(10):627–644, 2021.
3. Anjali Rao, Dalia Barkley, et al. Exploring tissue architecture using spatial transcriptomics. *Nature*, 596(7871):211–220, 2021.
4. Ludvig Larsson, Jonas Frisén, et al. Spatially resolved transcriptomics adds a new dimension to genomics. *Nature Methods*, 18(1):15–18, 2021.
5. Robert R Stickels, Evan Murray, et al. Highly sensitive spatial transcriptomics at near-cellular resolution with slide-seq2. *Nature Biotechnology*, 39(3):313–319, 2021.
6. Ao Chen, Sha Liao, et al. Spatiotemporal transcriptomic atlas of mouse organogenesis using dna nanoball-patterned arrays. *Cell*, 185(10):1777–1792, 2022.
7. Sheel Shah, Yodai Takei, et al. Dynamics and spatial genomics of the nascent transcriptome by intron seqfish. *Cell*, 174(2):363–376, 2018.
8. Jeffrey R Moffitt, Dhananjay Bambah-Mukku, et al. Molecular, spatial, and functional single-cell profiling of the hypothalamic preoptic region. *Science*, 362(6416):eaau5324, 2018.
9. Luyi Tian, Fei Chen, et al. The expanding vistas of spatial transcriptomics. *Nature Biotechnology*, 41(6):773–782, 2023.
10. Lucia Cassella and Anne Ephrussi. Subcellular spatial transcriptomics identifies three mechanistically different classes of localizing rnas. *Nature Communications*, 13(1):6355, 2022.
11. Chiara Baccin, Jude Al-Sabah, et al. Combined single-cell and spatial transcriptomics reveal the molecular, cellular and spatial bone marrow niche organization. *Nature Cell Biology*, 22(1):38–48, 2020.
12. Susanne C van den Brink, Anna Alemany, et al. Single-cell and spatial transcriptomics reveal somitogenesis in gastruloids. *Nature*, 582(7812):405–409, 2020.

13. Zhiwei Fan, Yangyang Luo, et al. Spascer: spatial transcriptomics annotation at single-cell resolution. *Nucleic Acids Research*, 51(D1):D1138–D1149, 2023.
14. Tommaso Biancalani, Gabriele Scalia, et al. Deep learning and alignment of spatially resolved single-cell transcriptomes with tangram. *Nature Methods*, 18(11):1352–1362, 2021.
15. Romain Lopez, Jeffrey Regier, et al. Deep generative modeling for single-cell transcriptomics. *Nature Methods*, 15(12):1053–1058, 2018.
16. Tamim Abdelaal, Soufiane Mourragui, et al. Spage: spatial gene enhancement using scrna-seq. *Nucleic Acids Research*, 48(18):e107–e107, 2020.
17. Chen Shengquan, Zhang Boheng, et al. stplus: a reference-based method for the accurate enhancement of spatial transcriptomics. *Bioinformatics*, 37(Supplement_1):i299–i307, 2021.
18. Zixuan Cang and Qing Nie. Inferring spatial and signaling relationships between cells from single cell transcriptomic data. *Nature Communications*, 11(1):2084, 2020.
19. Noa Moriel, Enes Senel, et al. Novosparc: flexible spatial reconstruction of single-cell gene expression with optimal transport. *Nature Protocols*, 16(9):4177–4200, 2021.
20. Xiaomeng Wan, Jiashun Xiao, et al. Integrating spatial and single-cell transcriptomics data using deep generative models with spatialscope. *Nature Communications*, 14(1):7848, 2023.
21. Kongming Li, Jiahao Li, et al. stdiff: a diffusion model for imputing spatial transcriptomics through single-cell transcriptomics. *Briefings in Bioinformatics*, 25(3):bbae171, 2024.
22. Xiang Zhou, Shihua Zhang, et al. Integrating spatial transcriptomics data across different conditions, technologies and developmental stages. *Nature Computational Science*, 3(10):894–906, 2023.
23. Jascha Sohl-Dickstein, Eric Weiss, et al. Deep unsupervised learning using nonequilibrium thermodynamics. In *International Conference on Machine Learning*, pages 2256–2265. PMLR, 2015.
24. Lvmin Zhang, Anyi Rao, et al. Adding conditional control to text-to-image diffusion models. In *Proceedings of the IEEE/CVF International Conference on Computer Vision*, pages 3836–3847, 2023.
25. Ilia Igashov, Hannes Stärk, et al. Equivariant 3d-conditional diffusion model for molecular linker design. *Nature Machine Intelligence*, pages 1–11, 2024.
26. Anoushka Joglekar, Andrey Prjibelski, et al. A spatially resolved brain region-and cell type-specific isoform atlas of the postnatal mouse brain. *Nature Communications*, 12(1):463, 2021.
27. Jeffrey R Moffitt, Dhananjay Bambah-Mukku, et al. Molecular, spatial, and functional single-cell profiling of the hypothalamic preoptic region. *Science*, 362(6416):eaau5324, 2018.
28. Nicholas Schaum, Jim Karkanias, et al. Single-cell transcriptomics of 20 mouse organs creates a tabula muris: The tabula muris consortium. *Nature*, 562(7727):367, 2018.
29. Xiao Wang, William E Allen, et al. Three-dimensional intact-tissue sequencing of single-cell transcriptional states. *Science*, 361(6400):eaat5691, 2018.
30. David W McKellar, Lauren D Walter, et al. Large-scale integration of single-cell transcriptomic data captures transitional progenitor states in mouse skeletal muscle regeneration. *Communications Biology*, 4(1):1280, 2021.
31. Sunny Z Wu, Ghamdan Al-Eryani, et al. A single-cell and spatially resolved atlas of human breast cancers. *Nature Genetics*, 53(9):1334–1347, 2021.
32. Oraly Sanchez-Ferras, Alain Pacis, et al. A coordinated progression of progenitor cell states initiates urinary tract development. *Nature Communications*, 12(1):2627, 2021.
33. Yan Zhou, Dong Yang, et al. Single-cell rna landscape of intratumoral heterogeneity and immunosuppressive microenvironment in advanced osteosarcoma. *Nature Communications*, 11(1):6322, 2020.
34. Alla Mikheenko, Andrey D Prjibelski, et al. Sequencing of individual barcoded cdnas using pacific biosciences and oxford nanopore technologies reveals platform-specific error patterns. *Genome Research*, 32(4):726–737, 2022.
35. Bin Li, Wen Zhang, et al. Benchmarking spatial and single-cell transcriptomics integration methods for transcript distribution prediction and cell type deconvolution. *Nature Methods*, 19(6):662–670, 2022.
36. William Peebles and Saining Xie. Scalable diffusion models with transformers. In *Proceedings of the IEEE/CVF International Conference on Computer Vision*, pages 4195–4205, 2023.
37. Jonathan Ho, Ajay Jain, and Pieter Abbeel. Denoising diffusion probabilistic models. In *Advances in Neural Information Processing Systems*, volume 33, pages 6840–6851, 2020.